*Journal of Sound and Vibration* (2003) **259**(3), 677–700
doi:10.1006/jsvi.2002.5099, available online at http://www.idealibrary.com on IDEAL®

# VORTEX-INDUCED VIBRATIONS OF TWO SIDE-BY-SIDE EULER-BERNOULLI BEAMS

R. M. C. So and X. Q. Wang

*Department of Mechanical Engineering, The Hong Kong Polytechnic University, Hung Hom, Kowloon, Hong Kong, China. E-mail: mmmcso@polyu.edu.hk*

(*Received* 20 *August* 2001, *and in final form* 11 *April* 2002)

Vortex-induced vibration of two side-by-side elastic beams in a cross flow is numerically studied. The two beams are identical and fixed at both ends. In the numerical approach, the Euler–Bernoulli beam theory is used to model the beam vibration, and the laminar Navier–Stokes equations are solved to give the flow field. The flow equations are resolved using a finite element method and the flow-induced forces are calculated at every time step in order to correctly reflect the fluid–beam interaction. The beam response is calculated using the modal analysis method. Free vibrations of the two beams with three pitch ratios, $T/D = 1{\cdot}13$, $1{\cdot}7$ and $3{\cdot}0$, where $T$ is the gap between the centers of the two beams and $D$ is the beam diameter, are simulated at $\mathrm{Re} = 800$. Results obtained are compared with experimental measurements and other numerical results obtained assuming a two-degree-of-freedom (2-d.o.f.) model. The agreement is good in general. Correlation analysis is carried out, showing that the phase relation is different for different $T/D$. The short-time Fourier transform (STFT) method is used to carry out the spectral analysis, along with the conventional auto-regressive moving averaging (ARMA) method for comparison. The STFT analysis shows that the time evolution of fluid force and beam vibration for $T/D = 1{\cdot}13$ and $3{\cdot}0$ are stationary. For these $T/D$ ratios, the STFT results are consistent with the ARMA results, but give a clearer picture of the higher order harmonics. For $T/D = 1{\cdot}7$, the time evolution is non-stationary. The STFT analysis shows that there are three types of frequency spectrum for the fluid force, with one, two, and three dominant frequencies respectively. The spectra intermittently change in a random way during the evolution. The ARMA results, though consistent with previous experiments, can only reveal a particular feature of the three different types of spectrum. This suggests that the STFT method is more appropriate to analyze the spectra of non-stationary time series in the study of flow-induced vibrations.



## 1. INTRODUCTION

Flow-induced vibration of two side-by-side beams is the simplest case of flow-induced vibration of beam arrays. In addition to fluid–structure interaction, the interaction between neighboring beams makes the flow field, and thus the fluid force and beam vibration, more complex than that of a single beam.

Two beams in a cross flow can be arranged in a side-by-side, tandem, and/or a staggered configuration, as illustrated in Figure 1. In the present study, the side-by-side arrangement of two cylindrical beams is considered. For such an arrangement, the pitch ratio $T/D$, where $T$ is the gap between the centers of two beams and $D$ is the beam diameter, is an important parameter. Zdravkovich [1, 2] has given excellent reviews of flow interference between two stationary beams for different values of $T/D$. When $T/D > 4$ , the interference is negligible and the wake of each beam is almost the same as the wake of a single beam. As $T/D$ is

0022-460X/02/$35.00 

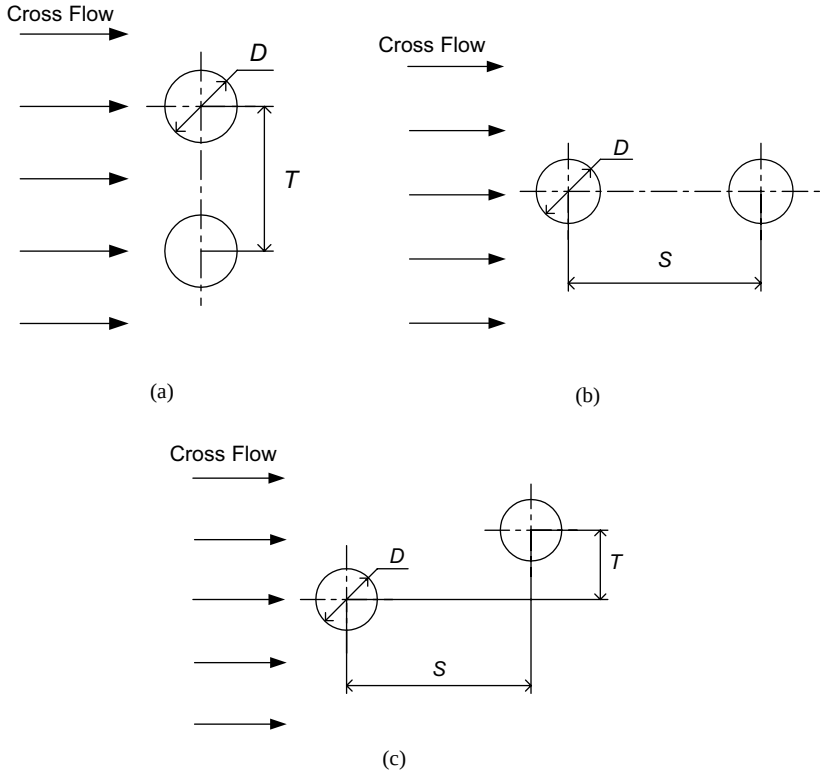


Figure 1. Illustration of various arrangements of two beams in a cross flow: (a) side-by-side; (b) tandem and (c) staggered.

reduced to the range, $2{\cdot}3 < T/D < 4$, two coupled vortex streets are observed. The two vortex streets have the same shedding frequency but are coupled in an out-of-phase mode. A further reduction of $T/D$ to between 1·1 and 2·3 gives rise to a biased flow pattern. Bearman and Wadcock [3] observed an asymmetric vortex street for this regime. The flow is bistable, intermittently changing over from one side to the other. Williamson [4] summarized the experimental data on the Strouhal number prior to his experiment, thus showing that three Strouhal numbers, around 0·1, 0·2 and 0·3, are associated with the two wakes. However, Kim and Durbin [5] reported only two Strouhal numbers for this regime. When $T/D$ is reduced to below 1·1, the two beams are strongly coupled and behave like a single bluff body. The observed asymmetry could be attributed to a near-wake phenomenon, rather than being related to the position of boundary layer separation.

When the beams are free to vibrate, the flow field becomes more complex because of fluid–structure interaction due to beam vibration [6, 7]. For two elastically supported rigid beams, the interference behavior can be classified into four regimes: negligible interference at $T/D > 4$, coupled vortex streets at $2{\cdot}2 < T/D < 4$, biased flow pattern at $1{\cdot}2 < T/D < 2{\cdot}2$, and single vortex street at $T/D < 1{\cdot}2$. The $T/D$ values separating different regimes are affected by system parameters such as the mass ratio, fluid damping, incoming flow, etc. Zhou *et al.* [8] experimentally investigated the interference behavior of two fixed–fixed elastic beams in a cross flow. Three pitch ratios, $T/D = 1{\cdot}13$, 1·7, and 3·0, were studied. It is shown that beam vibrations are essentially out of phase at $T/D = 1{\cdot}7$, while in phase at $T/D = 1{\cdot}13$. A significant finding is that synchronization occurs at several reduced velocities, corresponding to the first several natural frequencies of the system.

Numerical simulations of the flow-induced vibration of a relatively simple beam array are few compared with experimental measurements. Chang and Song [9] studied the interaction of vortex shedding of two beams at Re = 100, when $T/D = 1{\cdot}7$ and $3{\cdot}0$. For $T/D = 3{\cdot}0$, there are two types of vortex shedding, one is symmetric and the other is antisymmetric. The time series of the lift and drag coefficients are out of phase in the former case, but in phase in the latter case. The vortex shedding between these two types changes with time. For $T/D = 1{\cdot}7$, there is only one combined wake and the vortex shedding is asymmetric with a gap flow. Slaouti and Stansby [10] later investigated the flow around two stationary beams at Re = 200 for $T/D = 1{\cdot}1$, $1{\cdot}5$, and $3{\cdot}0$ using the random-vortex method, while Ng *et al.* [11] studied vortex interactions in the bistable flow regime at $T/D = 1{\cdot}75$. Unfortunately, Ng *et al.* [11] did not specify the Re of their calculations. On the other hand, Ichioka *et al.* [12] investigated the fluid–elastic vibration of two rigid beams at Re = 1000 for $T/D = 1{\cdot}5$. The two beams vibrate in a reverse phase mode. There is only one dominant frequency due to synchronization with the natural frequency of the beam. However, there is another frequency peak associated with each beam. In all these calculations, the beams are either stationary or the structural vibration is calculated assuming a two-degree-of-freedom (2-d.o.f.) model. Thus, both the flow field and the beam dynamics are modelled by invoking two-dimensional (2-D) assumptions. Seldom the Euler–Bernoulli beam theory is invoked to perform a 3-D calculation of the structural dynamics in a beam array. Consequently, vital information on the mode shape, natural frequencies of the different modes and their associated damping characteristics are not available.

Numerical simulation has not been performed so far for a pair of elastic beams in a cross flow, where the flow and the structures are assumed to be fully 3-D. As a first attempt, the flow around long slender beams could be assumed to be 2-D, however, the beam vibration can no longer be modelled by a spring–damper–mass system. Instead, the Euler–Bernoulli beam theory is used to resolve the 3-D vibration characteristics of the beams. This paper attempts a numerical simulation of the two-beam vibration problem at Re = 800. The calculated results are compared with experimental measurement [8]. A numerical approach developed by Wang *et al.* [13] for a single beam is extended to simulate this two-beam case. The behavior at $T/D = 1{\cdot}13$, $1{\cdot}7$, and $3{\cdot}0$ are calculated and compared with experimental measurements reported by Zhou *et al.* [8] and the numerical calculations of Liu *et al.* [14] assuming a 2-d.o.f. model for the beam dynamics. In addition to the use of an auto-regressive moving averaging (ARMA) technique [13–15] to analyze the stationary part of the time series, the short-time Fourier transform (STFT) method [16] is employed to analyze the time series in order to detect any non-stationary behavior.

## 2. THE NUMERICAL APPROACH

For flow-induced vibration problem with a single structure, four basic issues should be considered in any numerical simulation: modelling of the flow field, modelling of the structural vibration, modelling the fluid–structure interaction, and data analysis. In the case of multiple beams in a cross flow; an added complication is introduced by the beam–beam interaction. However, this particular aspect could be accounted for within the issue on modelling of fluid–structure interaction. Consequently, no additional issues are required for the simulation of free vibrations of multiple beams. These four issues for a single beam have been addressed and a numerical approach has been developed to treat a 3-D beam in a 2-D mean flow [13]. In the present study, the 2-D flow/3-D structure approach is extended to investigate vortex-induced vibration of two side-by-side beams. For the sake of

completeness, a brief description of each of these issues is given below. The interested reader is referred to references [13, 14, 17] for further details of the individual issues.

### 2.1. THE FLUID FLOW MODEL

A uniform cross flow of an incompressible, viscous Newtonian fluid around two elastic slender beams is considered. The upstream flow and the wake are assumed to be laminar and the beams are fixed at both ends. A justification for the laminar wake assumption in the Re range, $400 < \mathrm{Re} < 10000$, has been given in So *et al.* [17] and Wang *et al.* [13]. The governing laminar Navier–Stokes equations are

$$\frac{\partial \mathbf{u}}{\partial t} + (\mathbf{u}\cdot\nabla)\mathbf{u} = -\nabla p + \frac{1}{\mathrm{Re}}\nabla^2\mathbf{u}, \qquad \nabla\cdot\mathbf{u} = 0, \tag{1, 2}$$

where $\mathbf{u}$ is the dimensionless velocity vector normalized by the free-stream velocity $U_\infty$, $t = t^*U_\infty/D$ is the dimensionless time, $p$ is the dimensionless pressure normalized by $\rho U_\infty^2$, $\mathrm{Re} = U_\infty D/\nu$ is the Reynolds number, $D$ is the beam diameter, $\rho$ is the fluid density and $\nu$ is the fluid kinematic viscosity. The boundary and initial conditions can be specified as,

$$\mathbf{u}|_S = \mathbf{u}_b \quad \text{and} \quad \mathbf{u}|_{t=0} = \mathbf{u}_0 \tag{3}$$

where $S$ is the boundary of the domain $V$ occupied by the fluid.

The operator-splitting method [18] is used to solve the Navier–Stokes equations. The readers are referred to reference [18] for the detail of this method. Once the velocity and the pressure field has been obtained, the induced force on the structure is calculated using the following formula:

$$\mathbf{F}(z,t) = \oint\!\!\int \left( -p\mathbf{n} + \frac{1}{\mathrm{Re}}(\nabla\mathbf{u} + \nabla\mathbf{u}^{\mathrm{T}})\cdot\mathbf{n} \right) \Delta z \, \mathrm{d}s, \tag{4}$$

where the integration is performed around the circumference of the beam with arc length $s$ at each spanwise location $z$, $\Delta z$ is the elemental length along the span and $\mathbf{n}$ is the outward unit vector normal to the beam. The force vector, $\mathbf{F} = \{F_x, F_y\}$, consists of two components, the dimensionless unsteady drag (or streamwise) and lift (or transverse) forces respectively. Thus, the drag- and lift-force coefficients are defined as $C_D = 2F_x/(\rho U_\infty^2 \Delta z \pi D)$ and $C_L = 2F_y/(\rho U_\infty^2 \Delta z \pi D)$ respectively. All the calculated results are in the form of time series. From this point on, an overbar is used to denote the time average and a prime to designate the root mean square (r.m.s.) value of the signal. For example, the mean and r.m.s. values of $C_D$ are $\bar{C}_D$ and $C'_D$, respectively.

### 2.2. THE STRUCTURAL DYNAMICS MODEL

Each beam in the array is modelled by the Euler–Bernoulli beam theory and the modal analysis method is used to calculate the response of the beams in the present analysis [19].

The dynamic equation, made dimensionless by using the same parameters as those adopted for the Navier–Stokes equations, is expressed as

$$\ddot{\boldsymbol{\eta}}_m + 2\zeta_{sm}\left(\frac{2\pi}{U_{rm}}\right)\dot{\boldsymbol{\eta}}_{nm} + \left(\frac{2\pi}{U_{rm}}\right)^2 \boldsymbol{\eta}_m = \frac{\mathbf{F}_m}{M_r}, \tag{5}$$

where $U_{rm} = U_\infty/f^*_{nm}D = 1/f_{nm}$ is the reduced velocity corresponding to $f^*_{nm}$, the $m$th natural frequency of the beam, $f_{nm}$ is the dimensionless natural frequency, $M_r = m_b/\rho_f D^2$ is the mass

ratio, $m_b$ is the mass per unit length of the beam and $\rho_f$ is the fluid density. $\mathbf{F}_m$ is the $m$th mode generalized dimensionless force given by

$$\mathbf{F}_m(t) = \int W_m(z)\,\mathbf{F}(z,t)\,\mathrm{d}z, \quad m = 1, 2, \ldots, \tag{6}$$

where $W_m(z)$ is the $m$th normal mode of the undamped beam associated with the natural frequency $f^*_{nm}$,

The present beam model predicts both the transverse and the streamwise vibration of the beam along the span. In this sense, it accounts for the 3-D structural dynamics. The unsteady force vector, $\mathbf{F} = \{F_x, F_y\}$, is generally a function of time and the spanwise co-ordinate and, in principle, should be calculated based on a 3-D flow model. However, the flow field can be assumed 2-D for a long slender beam, that is, $\mathbf{F}$ is independent of the spanwise co-ordinate $z$. In such a way, the fluid forces at a cross-section of the beam can be calculated using the 2-D flow field enclosing that cross-section. The generalized force is thus expressed as

$$\mathbf{F}_m(t) = \int W_m(z)\,\mathbf{F}(t)\,\mathrm{d}z, \quad m = 1, 2, \ldots\ . \tag{7}$$

A fourth order Runge–Kutta method is used to solve equation (5). Once $\boldsymbol{\eta}_m(t)$ and $\dot{\boldsymbol{\eta}}_m(t)$ are evaluated, the dimensionless displacement and velocity of the beam are calculated using the following equations:

$$\mathbf{w}(z,t) = \sum_{m=1}^{N} W_m(z)\,\boldsymbol{\eta}_m(t), \qquad \dot{\mathbf{w}}(z,t) = \sum_{m=1}^{N} W_m(z)\,\dot{\boldsymbol{\eta}}_m(t). \tag{8a, b}$$

### 2.3. FLUID–BEAM AND BEAM–BEAM INTERACTION

From a computational point of view, flow-induced vibration is a moving boundary problem because the beam is free to move under the action of the flow-induced unsteady forces. The boundary of the computational domain changes with beam motion, and the no-slip boundary condition is applied on the surface of the beam. The mesh is deformed accordingly also. In order not to allow the mesh to deform to the extent that the boundary layer on the beam surface cannot be resolved properly, a Laplacian equation of displacement is solved to minimize the local mesh deformation. The Laplacian equation is expressed as

$$\nabla^2\boldsymbol{\delta} = 0, \tag{9}$$

and the boundary conditions given by $\boldsymbol{\delta} = 0$ at the outer boundary and $\boldsymbol{\delta} = \mathbf{w}$ at the boundary of the beam, where $\boldsymbol{\delta}$ is the deformation vector of the mesh nodes. The mesh is then remapped according to the deformation. In order to correctly account for the fluid–structure interaction, iteration is carried out within each time step until a stable status is reached. The readers are referred to So *et al.* [17] and Jadic *et al.* [20] for a detailed description of the process for a single beam and for a streamline body respectively.

### 2.4. DATA ANALYSIS

The time-marching approach gives the evolution of fluid force, beam vibration, flow velocity profile, etc. In order to understand the flow-induced vibration behavior, these data

TABLE 1

*Characteristic parameters of the two beams*

| $L$ (mm) | $D$ (mm) | $M_r$ | Natural frequencies (Hz), damping ratios, and dimensionless frequencies in still air | | | |
|---|---|---|---|---|---|---|
| 350·0 | 6·0 | 455·0 | $f_{n1}^* = 104$<br>$\zeta_{s1} = 0{\cdot}026$<br>$f_{10} = 0{\cdot}3013$ | $f_{n2}^* = 287$<br>$\zeta_{s2} = 0{\cdot}017$<br>$f_{20} = 0{\cdot}8316$ | $f_{n3}^* = 562$<br>$\zeta_{s3} = 0{\cdot}015$<br>$f_{30} = 1{\cdot}6284$ | $f_{n4}^* = 929$<br>$\zeta_{s4} = 0{\cdot}009$<br>$f_{40} = 2{\cdot}6918$ |

sets have to be analyzed to give the statistics, spectra, dominant frequencies and their associated damping characteristics. The ARMA method developed by Mignolet and Red-Horse [15] has been shown to be appropriate and has been successfully applied to perform spectral analysis of time series in experimental and numerical studies of flow-induced vibration of a single beam [20–23]. This same technique is used to analyze the time series if they are stationary. For non-stationary signals, the STFT method [16] is used to identify possible time-variant character.

The STFT method is essentially a windowed Fourier transform technique defined as

$$\mathrm{STFT}(t, \omega) = \int s(\tau)\gamma_{t,\omega}^*(\tau)\,\mathrm{d}\tau = \int s(\tau)\gamma^*(\tau - t)\,\mathrm{e}^{-\mathrm{j}\omega\tau}\,\mathrm{d}\tau, \tag{10}$$

where $s$ is the signal and $\gamma^*$ is called the window function. Similar to the frequency spectrum, the STFT spectrogram is defined as

$$SP(t, \omega) = |\mathrm{STFT}(t, \omega)|^2. \tag{11}$$

In order to analyze the time-variant behavior of the signal, the window function must be chosen so that one can get both local time and frequency characters. Usually the Gaussian function is used, expressed here as

$$\gamma^*(t) = \left(\frac{\alpha}{\pi}\right)^{1/4} \mathrm{e}(-\alpha/2)t^2 \tag{12}$$

where $\alpha$ is a coefficient which determines the degree of localization. The STFT spectrogram, as defined in equation (11), is a function of both frequency and time, thus reflecting time variation of the frequency spectrum of the non-stationary signal.

## 3. RESULTS AND DISCUSSION

Free vibrations of two elastic circular beams in a cross flow at $\mathrm{Re} = 800$ are simulated. For ease of identification, the beam on top is denoted as beam 1, while the other is designated as beam 2. Subscripts 1, 2, etc. will also be used to identify vibration modes. Their use will not confuse, but rather is self-explanatory based on the variable considered. The two beams are identical, of finite length, and fixed at both ends. The first four natural frequencies of the two beams and their geometric dimensions are listed in Table 1. Here, the dimensional natural frequency is denoted by $f_{ni}^*$, while the dimensionless natural frequency is designated by $f_{io}$, where $i = 1, 2, 3$, etc. is used to indicate the vibration mode. Only the structural damping ratio, $\zeta_s$, is reported because there is no other damping in the system when the beams are exposed to still air.

The vibrations of the beams at three pitch ratios, $T/D = 1{\cdot}13$, $1{\cdot}70$, and $3{\cdot}0$, are studied in the numerical simulation. These are three representative $T/D$ values for the regime of a single vortex street, the regime of biased flow, and the regime of two coupled-vortex-streets, respectively, for two side-by-side beams. This choice is motivated by the desire to understand how free vibration of the beams affect the wake flow and, in turn, the beam dynamics. In this kind of arrangement, the free vibration of the beams will give rise to two interaction effects, fluid–beam and beam–beam interaction. The objective of the present study attempts to assess the effect of these two different types of interaction. The statistics of the fluid forces and beam displacements at mid-span are also calculated in order to compare with experimental measurement [8] and numerical results obtained from a 2-d.o.f. modelling of the same problem [14]. In addition, the vibration modes and possible correlation along the span of the beams are examined in order to seek understanding of the fluid–beam and beam–beam interaction effects.

### 3.1. THE $T/D = 3{\cdot}0$ CASE

For this $T/D$, the two vortex streets are coupled. Whether this will give rise to non-stationary behavior in the wake remains to be seen. The calculated time series of the force coefficients and beam displacements are plotted in Figure 2. In these and other subsequent plots, the ordinate is the normalized time, $t$. These time series are very similar to those calculated for a single beam [13], and they appear to approach a stationary behavior after a finite time. This means that the time series can be first analyzed assuming them to be stationary and then further examined for time-variant behavior.

Data analysis is carried out over a finite period of the stationary time series. Firstly, the statistics are calculated and listed in Table 2 for comparison with available experimental measurements and numerical results obtained from a 2-d.o.f. model. Only the statistics of the force coefficients, $C_D$ and $C_L$, and those of the displacements, $X$ and $Y$, are shown. As before, the subscripts 1 and 2 are used to denote the location of the beams, 1 on top and 2 below. Measurements of $\bar{C}_D$ and $\bar{C}_L$ for both beams and $Y$ for beam 1 have been reported at the mid-span of the beams. Comparisons are made with these measurements. For this case, $\bar{C}_L$ should be close to zero. Both numerical models yield results that are very close to zero, but the measurements give a finite, though small value. The calculations indicate that the beams are repulsive but the measurements show that they move in unison. However, the physics seems to support the calculations. The calculated $\bar{C}_D$ is in approximate agreement with the numerical and experimental data; the present result being the largest while the measurement is the smallest. This is true for both beams because, at this $T/D$, the drag is the same for both. The calculated $Y_1'$ is three plus times larger than the experimental measurement, but is only about 15% larger than the result obtained from a 2-d.o.f. model. The discrepancy between the numerical results is due to the fact that a 2-d.o.f. model cannot account for the contribution of the higher modes. The discrepancy between measurement and calculation is a direct consequence of the disagreement noted in $\bar{C}_L$.

Secondly, a correlation analysis is carried out. The correlation coefficient, $\Lambda(P, Q)$, is calculated to study the phase relation between $C_L$, $C_D$ and $Y$, $X$ of the two beams. The correlation coefficient is defined as

$$\Lambda(P, Q) = E[(P - \mu_P)]E[(Q - \mu_Q)]/(\sigma_P \sigma_Q), \tag{13}$$

where $P$ and $Q$ are the time series of two signals, $\mu$ is the mean and $\sigma$ is the standard deviation of the signal. In the lift direction, the correlation coefficients of $C_L$ and $Y$ for the two beams are identical and equal to $-0{\cdot}9998$. This suggests that $C_L$ and $Y$ be out of phase.

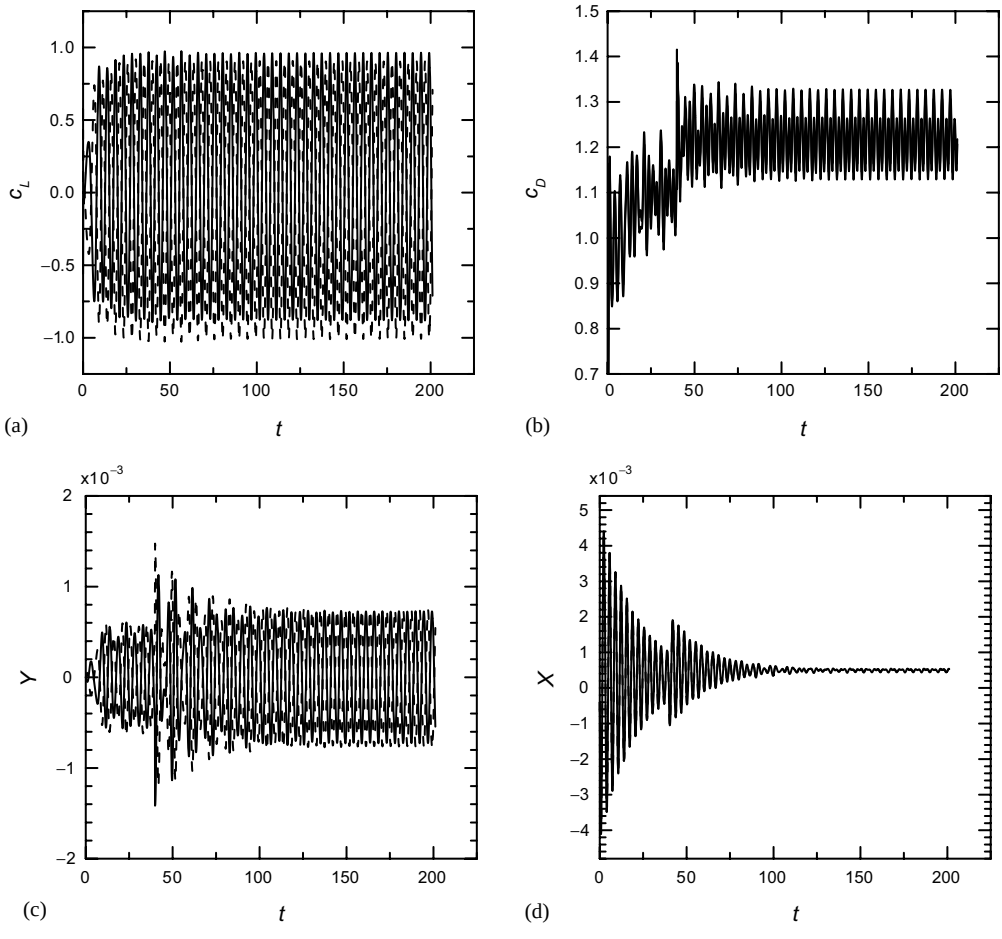


Figure 2. Time evolution of fluid forces and beam displacements for the $T/D = 3{\cdot}0$ case: (a) $C_L$; (b) $C_D$; (c) $Y$; (d) $X$; ——, beam 1; ------, beam 2.

In the streamwise direction, the correlation coefficients of $C_D$ and $X$ between the two beams are 0·9964 and 0·9972, respectively, thus suggesting an in-phase relation between the two beams. This is consistent with previous experimental result [8].

For this $T/D$, the fluid force and beam displacement time series are approximately sinusoidal. First, the ARMA technique is used to analyze them. The calculated frequency spectra of $C_L$ and $C_D$ for both beams are shown in Figure 3. From this point on, the ordinate of all spectral plots is the dimensionless frequency, $f$. The two beams have almost the same frequency spectrum. There is only one dominant vortex shedding frequency in the spectra of $C_L$ and it is occurring at approximately $f = 0.21$ for both beams (Figure 3(a)). This also is the Strouhal number. For the spectra of $C_D$, there are two dominant frequencies, one occurring at $f = 0{\cdot}21$ and another at $f = 0{\cdot}42$ (Figure 3(b)). The latter is the dominant frequency of the fluctuating drag and is exactly double that of the vortex shedding frequency.

In order to ascertain that the time series are indeed stationary, a STFT analysis is carried out at several selected time locations within one period of time evolution of the fluctuating lift force as shown in Figure 4(a). The calculated spectrograms are shown in Figure 4(b). It is seen that the frequency spectrum essentially does not change with time, suggesting that the

TABLE 2

*Comparison of numerical calculations with experimental measurements for the case, $T/D = 3{\cdot}0$*

| | Present result | Numerical result from 2-d.o.f. model [14] | Experimental measurements [8] |
|---|---|---|---|
| $\bar{C}_{L1}$ | 0·0258 | 0·08 | 0·14 |
| $\bar{C}_{L2}$ | − 0·0381 | − 0·08 | 0·02 |
| $C'_{L1}$ | 0·6484 | — | — |
| $C'_{L2}$ | 0·6740 | — | — |
| $\bar{C}_{D1}$ | 1·2097 | 1·15 | 1·07 |
| $\bar{C}_{D2}$ | 1·2290 | 1·15 | 1·07 |
| $C'_{D1}$ | 0·0538 | — | — |
| $C'_{D2}$ | 0·0555 | — | — |
| $\bar{Y}_1$ | $1{\cdot}0957 \times 10^{-5}$ | — | — |
| $\bar{Y}_2$ | $-1{\cdot}5882 \times 10^{-5}$ | — | — |
| $Y'_1$ | $5{\cdot}1469 \times 10^{-4}$ | $4{\cdot}5 \times 10^{-4}$ | $1{\cdot}5 \times 10^{-4}$ |
| $Y'_2$ | $5{\cdot}3468 \times 10^{-4}$ | — | — |
| $\bar{X}_1$ | $4{\cdot}9746 \times 10^{-4}$ | — | — |
| $\bar{X}_2$ | $5{\cdot}0537 \times 10^{-4}$ | — | — |
| $X'_1$ | $2{\cdot}9839 \times 10^{-5}$ | — | — |
| $X'_2$ | $2{\cdot}9589 \times 10^{-5}$ | — | — |

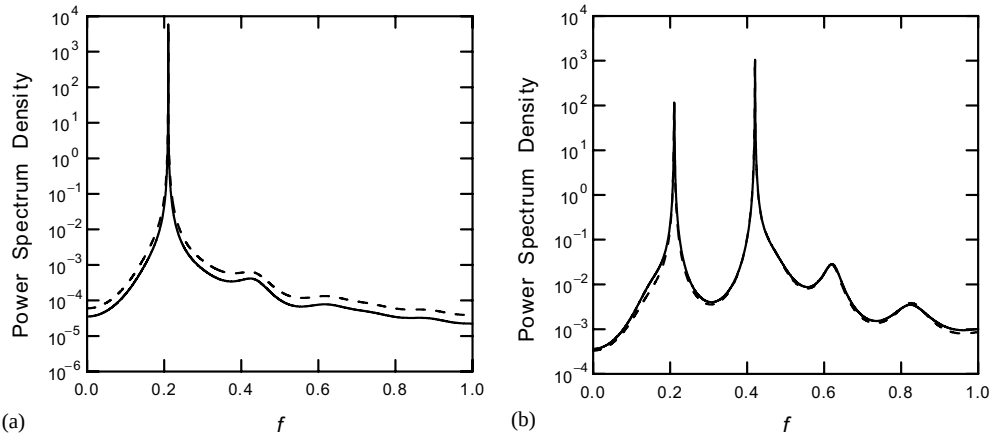


Figure 3. The spectra of fluid forces for the $T/D = 3{\cdot}0$ case deduced using ARMA: (a) $C_L$; (b) $C_D$; ——, beam 1; ------, beam 2.

time evolution of the fluctuating lift is a stationary process. In Figure 5(a) is plotted a comparison of the STFT and ARMA results. It can be seen that the STFT analysis identifies higher harmonics at both odd and even orders, which are not very obvious in the ARMA spectrum. This feature is different from that observed in a freely vibrating single beam. The STFT and ARMA results of a single beam at $\mathrm{Re} = 994$ are also plotted in Figure 5(b) for comparison. Higher harmonics only occur at odd orders in the case of a single beam. Thus, it can be seen that beam–beam interaction gives rise to the higher harmonics at even orders for this $T/D$.

The next step is to examine the $X$ and $Y$ time series to see if the same behavior as the $C_D$ and $C_L$ time series is observed. The frequency spectra of $X$ and $Y$ obtained using the

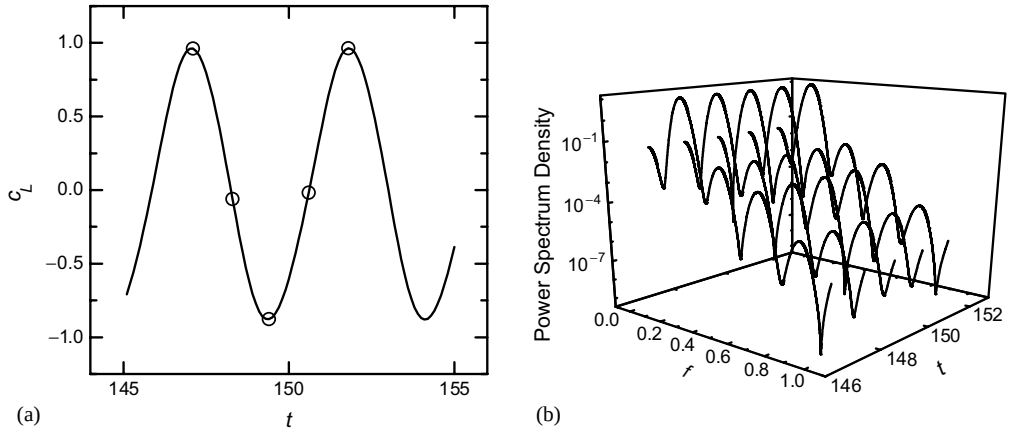


Figure 4. The STFT spectral analysis of $C_{L1}$ for the $T/D = 3{\cdot}0$ case: (a) illustration of the time points at which the STFT analysis is carried out; (b) STFT spectrograms.

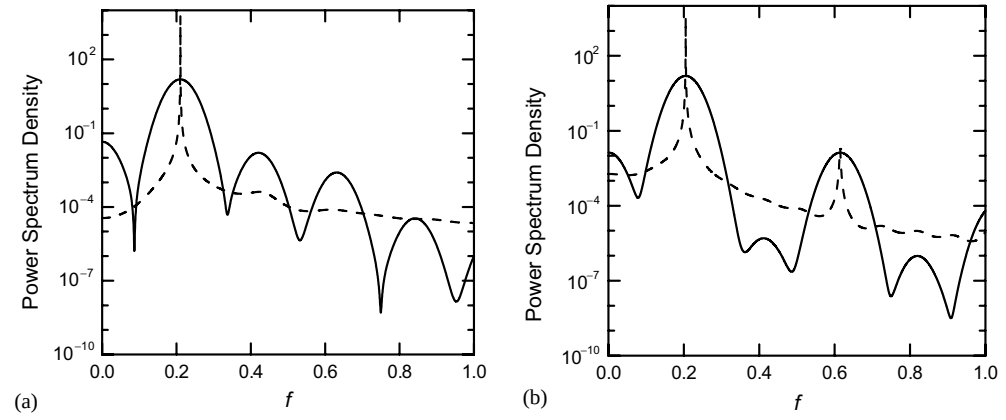


Figure 5. STFT and ARMA spectrum of $C_L$ for: (a) beam 1 of the $T/D = 3{\cdot}0$ case, (b) single beam; ——, STFT spectrogram; - - - - - -, ARMA spectrum.

ARMA method are plotted in Figure 6. These spectra show that the two beams are responding to the fluid forces at the dominant excitation frequency, i.e., $f = 0{\cdot}21$. The time-variant spectrograms are given in Figure 7, showing that the $X$ and $Y$ time series are also stationary. A comparison of the STFT and ARMA results is given in Figure 8. It can be seen that higher harmonics occur at both odd and even orders, just like the force signals.

### 3.2. THE $T/D = 1{\cdot}13$ CASE

At this $T/D$, the beam wakes merge to form a single vortex street [1–4]. The calculated $C_L$, $C_D$, $Y$ and $X$ time series are shown in Figure 9. Similar to the $T/D = 3{\cdot}0$ case, where the two vortex streets are coupled, it is noticed that the time series again approach stationary behavior after a finite time and appear to be periodic although not sinusoidal. Again, a set of data is chosen from the stationary part of the calculated time series for analysis. The statistics thus obtained are listed in Table 3 for comparison with experimental measurement

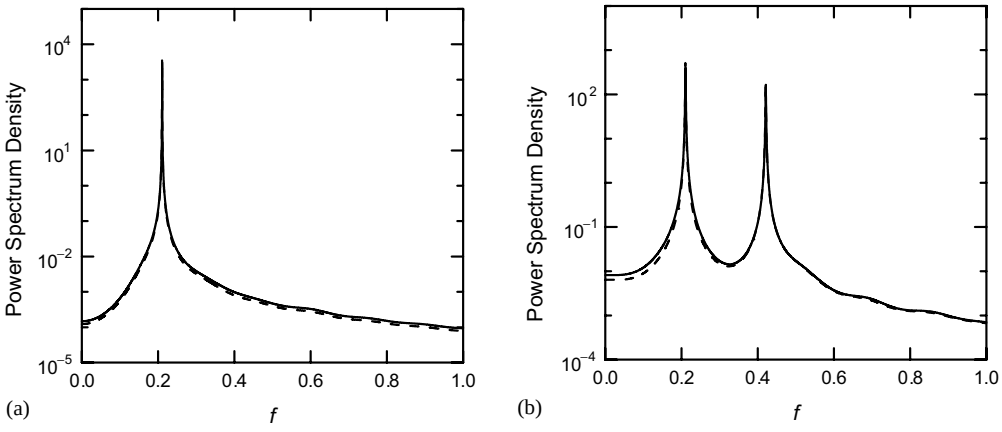


Figure 6. The ARMA calculated spectra of beam displacements for the $T/D = 3{\cdot}0$ case: (a) $Y$; (b) $X$; ——, beam 1; ------, beam 2.

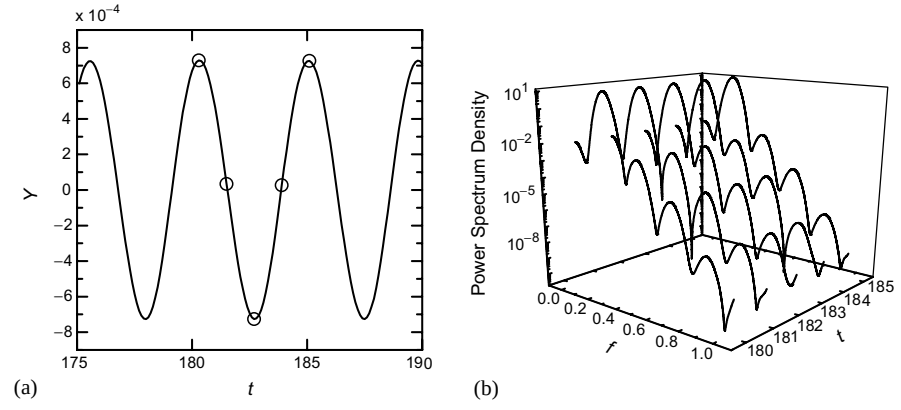


Figure 7. The STFT spectral analysis of $Y_1$ for the $T/D = 3{\cdot}0$ case: (a) illustration of the time points at which the STFT analysis is carried out; (b) STFT spectrograms.

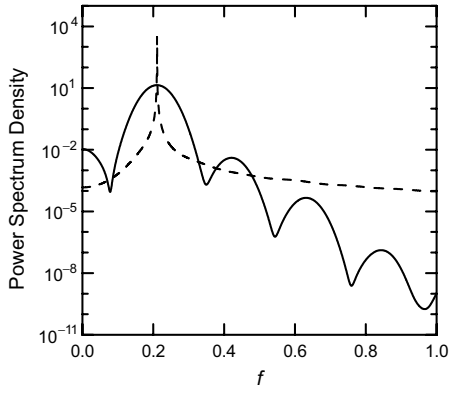


Figure 8. STFT and ARMA spectrum of $Y_1$ for the $T/D = 3{\cdot}0$ case: ——, STFT spectrogram; ------, ARMA spectrum.

TABLE 3

*Comparison of numerical calculations with experimental measurements for the case,* $T/D = 1{\cdot}13$

| | Present result | Numerical result from 2-d.o.f. model [14] | Experimental measurements [8] |
|---|---|---|---|
| $\bar{C}_{L1}$ | 0·6654 | 0·65 | 0·52 |
| $\bar{C}_{L2}$ | − 0·6726 | − 0·67 | − 0·48 |
| $C'_{L1}$ | 0·7820 | — | — |
| $C'_{L2}$ | 0·7824 | — | — |
| $\bar{C}_{D1}$ | 1·9878 | 1·93 | 1·10 |
| $\bar{C}_{D2}$ | 1·9766 | 1·93 | 0·95 |
| $C'_{D1}$ | 0·3184 | — | — |
| $C'_{D2}$ | 0·3155 | — | — |
| $\bar{Y}_1$ | $2{\cdot}7375 \times 10^{-4}$ | — | — |
| $\bar{Y}_2$ | $-2{\cdot}7643 \times 10^{-4}$ | — | — |
| $Y'_1$ | $5{\cdot}4036 \times 10^{-4}$ | $2{\cdot}0 \times 10^{-4}$ | $2{\cdot}3 \times 10^{-4}$ |
| $Y'_2$ | $5{\cdot}3939 \times 10^{-4}$ | — | — |
| $\bar{X}_1$ | $8{\cdot}1739 \times 10^{-4}$ | — | — |
| $\bar{X}_2$ | $8{\cdot}1466 \times 10^{-4}$ | — | — |
| $X'_1$ | $2{\cdot}6586 \times 10^{-4}$ | — | — |
| $X'_2$ | $2{\cdot}6977 \times 10^{-4}$ | — | — |

and the numerical result of a 2-d.o.f. structural model. The calculated $\bar{C}_D$ is the same for both beams, in agreement with the 2-d.o.f. results and approximately with measurements. As for $\bar{C}_L$, a repulsive behavior is predicted, and this trend is in agreement with experiments and the 2-d.o.f. results. The predictions are in quantitative agreement with the 2-d.o.f. calculations and agree much better with measurements, contrary to the $T/D = 3{\cdot}0$ case. The prediction of $Y'_1$ is still larger than the other two sets of data, but not as much as in the $T/D = 3{\cdot}0$ case. For this $T/D$, $\bar{C}_L$ is non-zero; this non-zero mean-value suggests an asymmetric pressure distribution about the $x$-axis, as observed in the experiment [8].

The correlation coefficient of $C_L$ between the two beams is $\Lambda = 0{\cdot}5183$. This suggests a phase difference of $0{\cdot}33\pi$ for the fluid forces of the two beams. The correlation coefficient of $Y$ between the two beams is $\Lambda = -0{\cdot}2156$, and the phase difference is $0{\cdot}57\pi$. This is quite different from that deduced from $C_L$ and can be attributed to the difference in response of the beams. It should be noted that the phase difference between $C_L$ when the two beams are static is $0{\cdot}34\pi$ ($\Lambda = 0{\cdot}4783$), that is, beam vibration does not alter the phase relationship between the fluctuating forces acting on the two beams. The difference between the correlation coefficients of $C_L$ and $Y$ can be due to the presentation of the response at the natural frequency of the beam. A calculation of the correlation coefficient between $C_L$ and $Y$ shows that the phase difference is around $0{\cdot}17\pi$. This suggests that the beam is responding to the excitation force at different frequencies. The behavior will be made clearer when the frequency spectra of $C_L$ and $Y$ are examined later.

The frequency spectra of $C_L$ and $C_D$ calculated using the ARMA method are plotted in Figure 10. It is seen that there are two Strouhal numbers, one is 0·12 and another is 0·25. This has been reported previously for a pitch ratio around 1·25 [3, 4]. While the Strouhal number of 0·25 can be considered similar to that found in a single beam, So *et al.* [23] has shown that the additional Strouhal number 0·12 is due to the effect of gap flow. It is also seen that an even order higher harmonics at $f = 0{\cdot}49$ is quite prominent. The STFT spectrogram shown in Figure 11 clearly demonstrates that higher harmonics occur at even

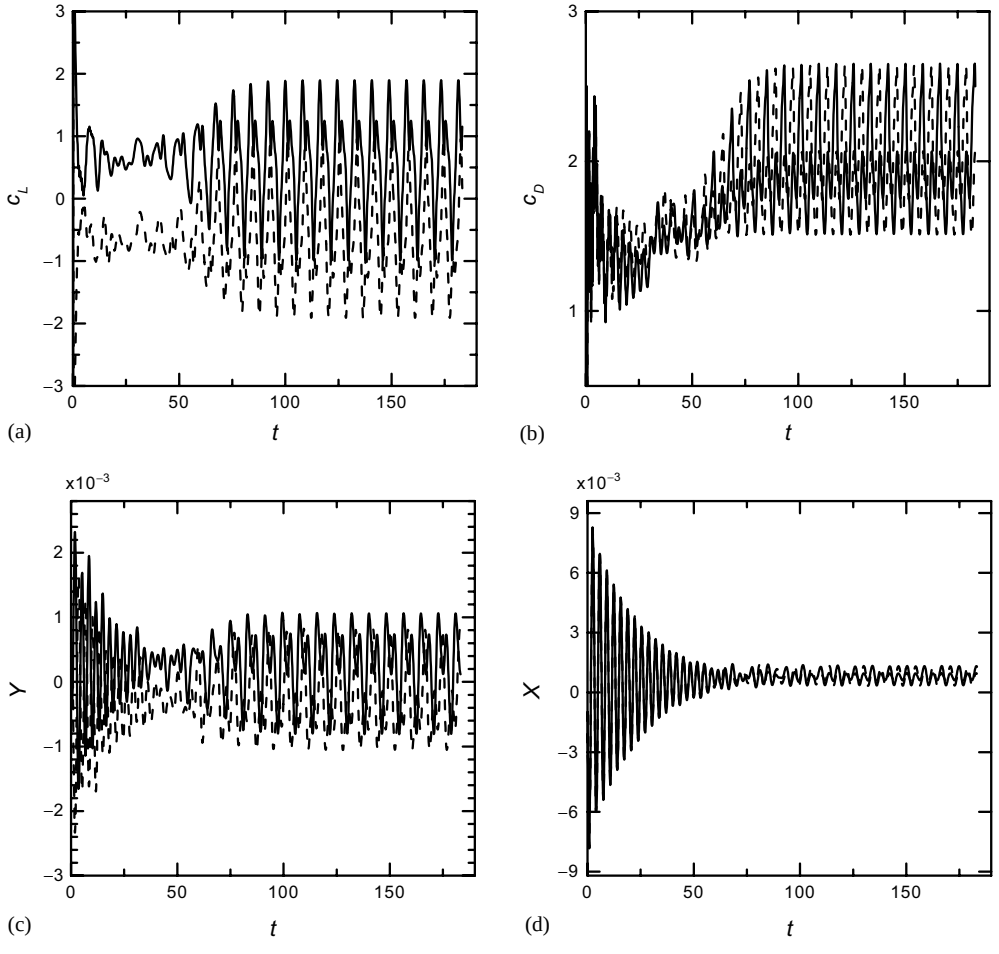


Figure 9. Time evolution of fluid forces and beam displacements for the $T/D = 1{\cdot}13$ case: (a) $C_L$; (b) $C_D$; (c) $Y$; (d) $X$; ——, beam 1; ------, beam 2.

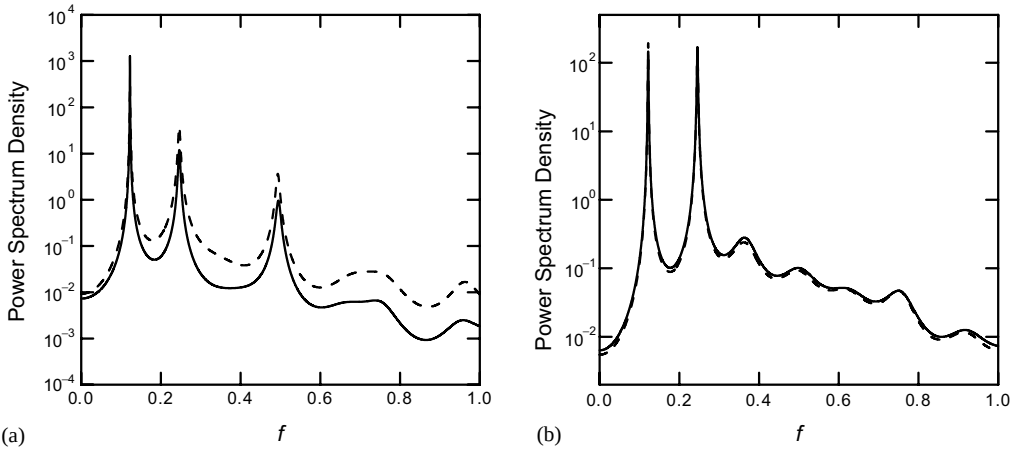


Figure 10. The spectra of fluid forces for the $T/D = 1{\cdot}13$ case deduced using ARMA: (a) $C_L$; (b) $C_D$; ——, beam 1; ------, beam 2.

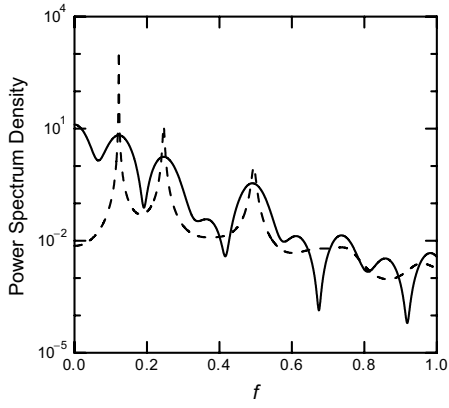


Figure 11. STFT and ARMA spectrum of $C_L$ for: (a) beam 1 of the $T/D = 1{\cdot}13$ case: (b) single beam; ——, STFT spectrogram; - - - - - -, ARMA spectrum.

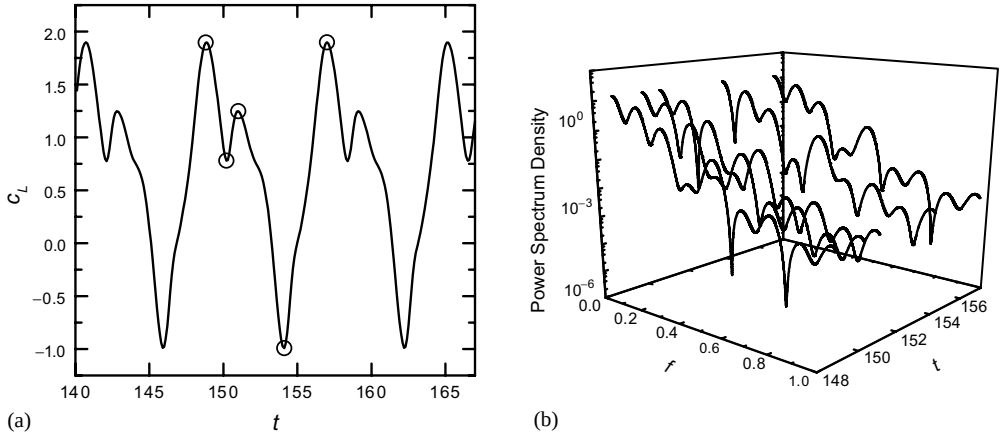


Figure 12. The STFT spectral analysis of $C_{L1}$ for the $T/D = 1{\cdot}13$ case: (a) illustration of the time points at which the STFT analysis is carried out; (b) STFT spectrograms.

orders. This is different from the case of a single beam and the case of two beams at $T/D = 3{\cdot}0$. The STFT spectrograms at several selected time locations within one period of time evolution of the fluid force are plotted in Figure 12. It is found that although the main feature of the frequency spectrum does not change with time, it is not difficult to observe its variation in form with time. This indicates that the time evolution of the fluctuating forces is a slightly non-stationary process. This time variation is clearly shown in the STFT analysis of the beam displacements.

The frequency spectra of $Y$ and $X$ calculated using the ARMA method are shown in Figure 13. Apart from the response at the frequencies of $f = 0{\cdot}12$, $0{\cdot}25$, and $0{\cdot}50$, it can be seen that a response peak also occurs at $f = 0{\cdot}36$. This peak can be attributed to the first mode of vibration of the two beams whose natural frequency in still air is $0{\cdot}30$. Compared with the frequency spectra of $C_L$ and $C_D$, the response at $f = 0{\cdot}25$ is higher while that at $f = 0{\cdot}50$ is lower. This may contribute to the phase difference between beam vibration and the fluctuating force. The response at the first natural frequency of the beam can be clearly seen in the STFT spectrogram comparison with the corresponding ARMA result for

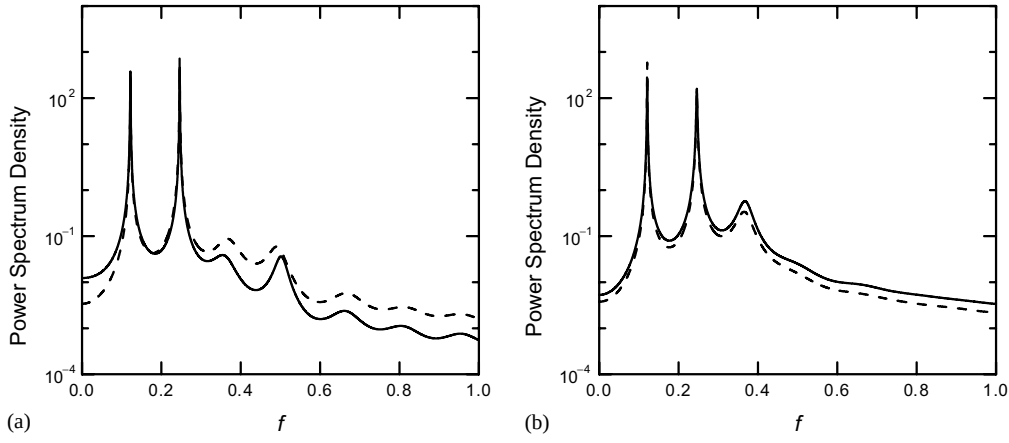


Figure 13. The ARMA calculated spectra of beam displacements for the $T/D = 1{\cdot}13$ case: (a) $Y$, (b) $X$; ——, beam 1; - - - - - -, beam 2.

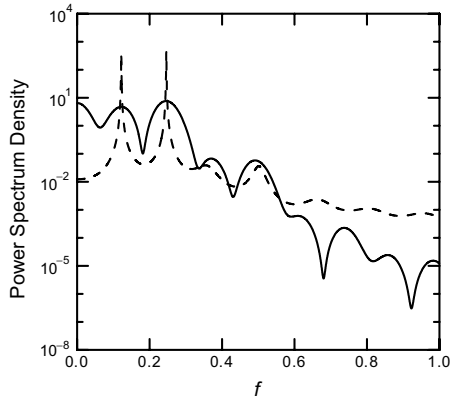


Figure 14. STFT and ARMA spectrum of $Y_1$ for the $T/D = 1{\cdot}13$ case: ——, STFT spectrogram; - - - - - -, ARMA spectrum.

$Y_1$ (Figure 14). The STFT spectrograms at several selected time locations within one period of time evolution of $Y$ are plotted in Figure 15. It can be seen that the response at the first natural frequency, $f = 0{\cdot}36$, shows obvious variation with time, hence, the slightly non-stationary behavior of the fluctuating forces and beam responses.

### 3.3. THE $T/D = 1{\cdot}7$ CASE

For two side-by-side rigid beams in a cross flow, a biased flow pattern exists in the wake for the $T/D = 1{\cdot}7$ case. The same has also been observed in the two elastic beams experiment [8]. This gives rise to non-stationary time series for the forces and the beam displacements. In order to demonstrate that this is indeed the case, the calculated time series of the fluctuating forces and beam displacements for the $T/D = 1{\cdot}7$ case is plotted in Figure 16. They are quite different from those presented in the $T/D = 1{\cdot}13$ and $3{\cdot}0$ cases, where a single vortex street and two coupled vortex streets are observed respectively. The time

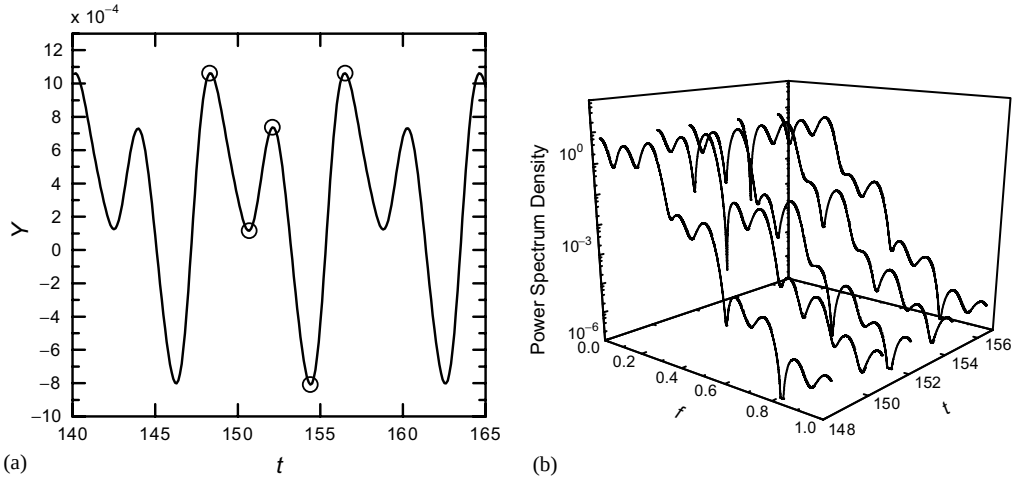


Figure 15. The STFT spectral analysis of $Y_1$ for the $T/D = 1{\cdot}13$ case: (a) illustration of the time points at which the STFT analysis is carried out; (b) STFT spectrograms.

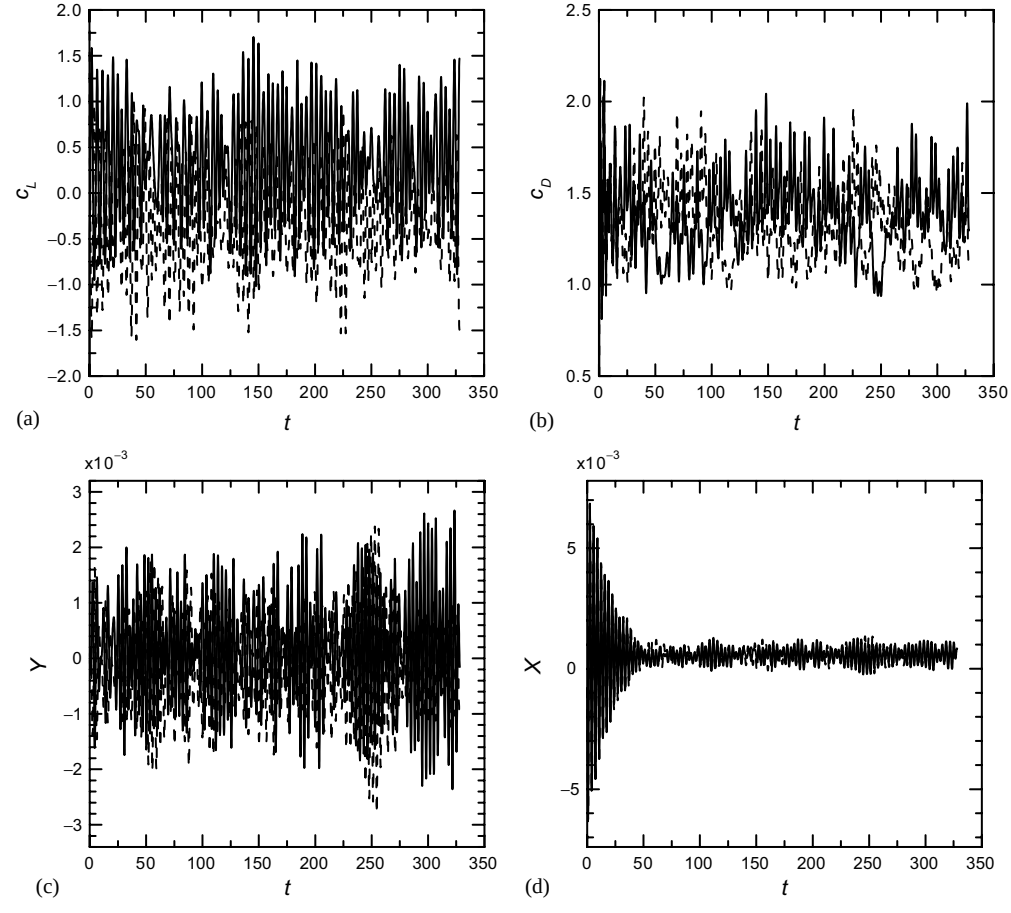


Figure 16. Time evolution of fluid forces and beam displacements for the $T/D = 1{\cdot}7$ case: (a) $C_L$; (b) $C_D$: (c) $Y$; (d) $X$; ——, beam 1; - - - - - -, beam 2.

TABLE 4

*Comparison of numerical calculations with experimental measurements for the case, $T/D = 1{\cdot}7$*

| | Present result | Numerical result from 2-d.o.f. model [14] | Experimental measurements [8] |
|---|---|---|---|
| $\bar{C}_{L1}$ | 0.26–0.38 | 0.30 | 0.37 |
| $C'_{L1}$ | 0.38–0.74 | — | — |
| $\bar{Y}_1$ | 0.9–1.6 ($\times 10^{-4}$) | — | — |
| $Y'_1$ | 7.3–11.1($\times 10^{-4}$) | $10{\cdot}5 \times 10^{-4}$ | $4.0 \times 10^{-4}$ |

series do not approach a stationary state and are not periodic. Therefore, it is expected that the statistics and the correlation are time variant, and the ARMA method is inadequate for this set of data. In view of this, the STFT method is used to carry out the spectral analysis, while the ARMA method is applied to the complete time series to give an overall frequency spectrum. The statistics are calculated and the correlation analysis is carried out on a time-variant basis, i.e., the non-stationary nature of the signals is taken into account. Statistics thus obtained, expressed in the form of a range to represent such a time-variant nature, are listed in Table 4 for comparison with experimental measurements and numerical results of the 2-d.o.f. structural model. The prediction of lift coefficients is good, but the calculated transverse displacement is larger than the experimental result. Noting that the numerical approach using a 2-d.o.f. structural model gives similar results, this suggests that the present approach needs further improvements in the modelling of fluid flow.

The time-variant STFT spectrograms of $C_L$ and $Y$ for beam 1 are shown in Figure 17. In order to demonstrate the time variation of the frequency content, a series of 2-D plots at different $t$ are given instead of a comprehensive 3-D plot.

At $t = 20$, there is only one dominant frequency at $f = 0{\cdot}23$ for $C_L$. This behavior is similar to that found in the case of two coupled-vortex-streets, but the dominant frequency is slightly higher. There is also a small peak at $f = 0{\cdot}72$, approximately three times that given by $f = 0{\cdot}23$, and no even order harmonics are observed. For the corresponding $Y$, two peaks at $f = 0{\cdot}23$ and 0·30 can be identified, the former corresponding to the excitation frequency while the latter to the first natural frequency of the beam.

When the flow further develops, the time evolution of $C_L$ becomes unstable. At $t = 40$, the dominant frequency of $C_L$ has shifted to $f = 0{\cdot}20$, and two peaks appear, one at $f = 0{\cdot}10$ and another at $f = 0{\cdot}28$, although they are not quite as discernible. Higher order harmonics are observed. As for $Y$, the dominant frequency occurs at $f = 0{\cdot}31$ which is the first natural frequency of the beam, and there are two smaller peaks occurring at $f = 0{\cdot}10$ and 0·22, corresponding to the excitation frequencies. At $t = 60$, the frequency at $f = 0{\cdot}20$ disappears and two dominant frequencies at $f = 0{\cdot}13$ and 0·25 begin to show in the $C_L$ spectrogram. In the $Y$ spectrogram, the dominant frequency still occurs at $f = 0{\cdot}30$, while there is a smaller peak at $f = 0{\cdot}14$.

The frequency content then shifts back to the behavior with one dominant frequency at $f = 0{\cdot}21$, as shown in the spectrograms of $C_L$ at $t = 80$ and 100. At $t = 120$, three dominant frequencies appear at $f = 0{\cdot}16$, 0·21, and 0·30. This behavior is very much like that observed at $t = 40$. As time increases to $t = 140$, the frequency peak at $f = 0{\cdot}30$ disappears and there remains two dominant frequencies at $f = 0{\cdot}11$ and 0·22. The dominant frequency of $Y$ also occurs at $f = 0{\cdot}22$. The two frequency peaks in $C_L$ shift to $f = 0{\cdot}14$ and 0·24 at $t = 160$, and the corresponding $Y$ spectrogram shows two dominant frequencies at $f = 0{\cdot}24$ and 0.31. At

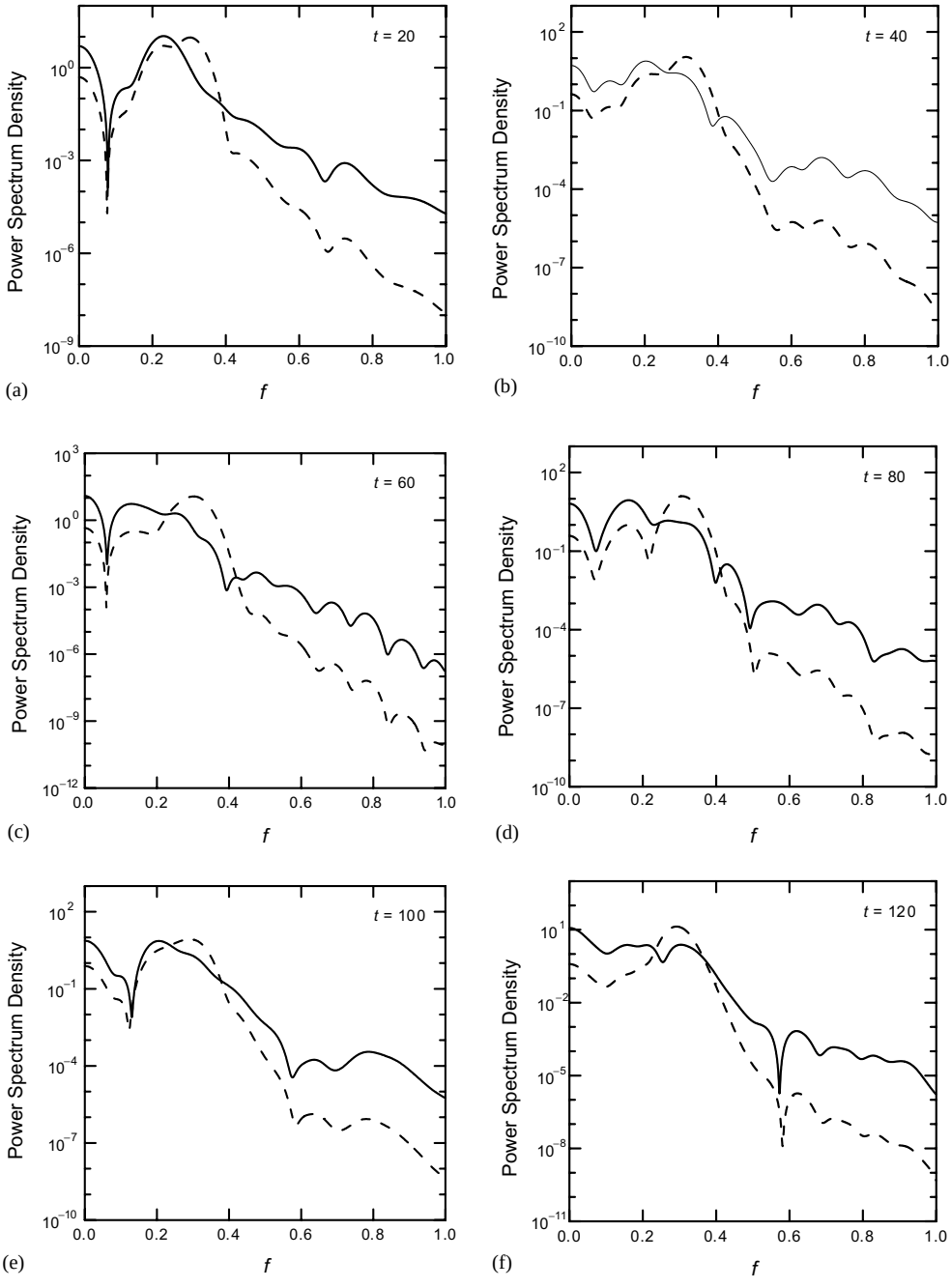


Figure 17. The STFT spectral analysis of $C_{L1}$ and $Y_1$ for the $T/D = 1.7$ case: $C_{L1}$; ——, $Y$; – – –.

$t = 180$, two dominant frequencies can still be found in the $C_L$ spectrogram, but they occur at $f = 0{\cdot}21$ and $0{\cdot}31$, and the $Y$ spectrogram also show peaks at these two frequencies. As time increases further to $t = 200$, the frequency at $f = 0{\cdot}31$ disappears and the peak at $f = 0{\cdot}21$ slightly shifts to $0{\cdot}23$. Thus, the frequency content of the spectrum at this moment is almost the same as that at $t = 20$. At $t = 220$, the dominant frequency remains at $f = 0{\cdot}21$,

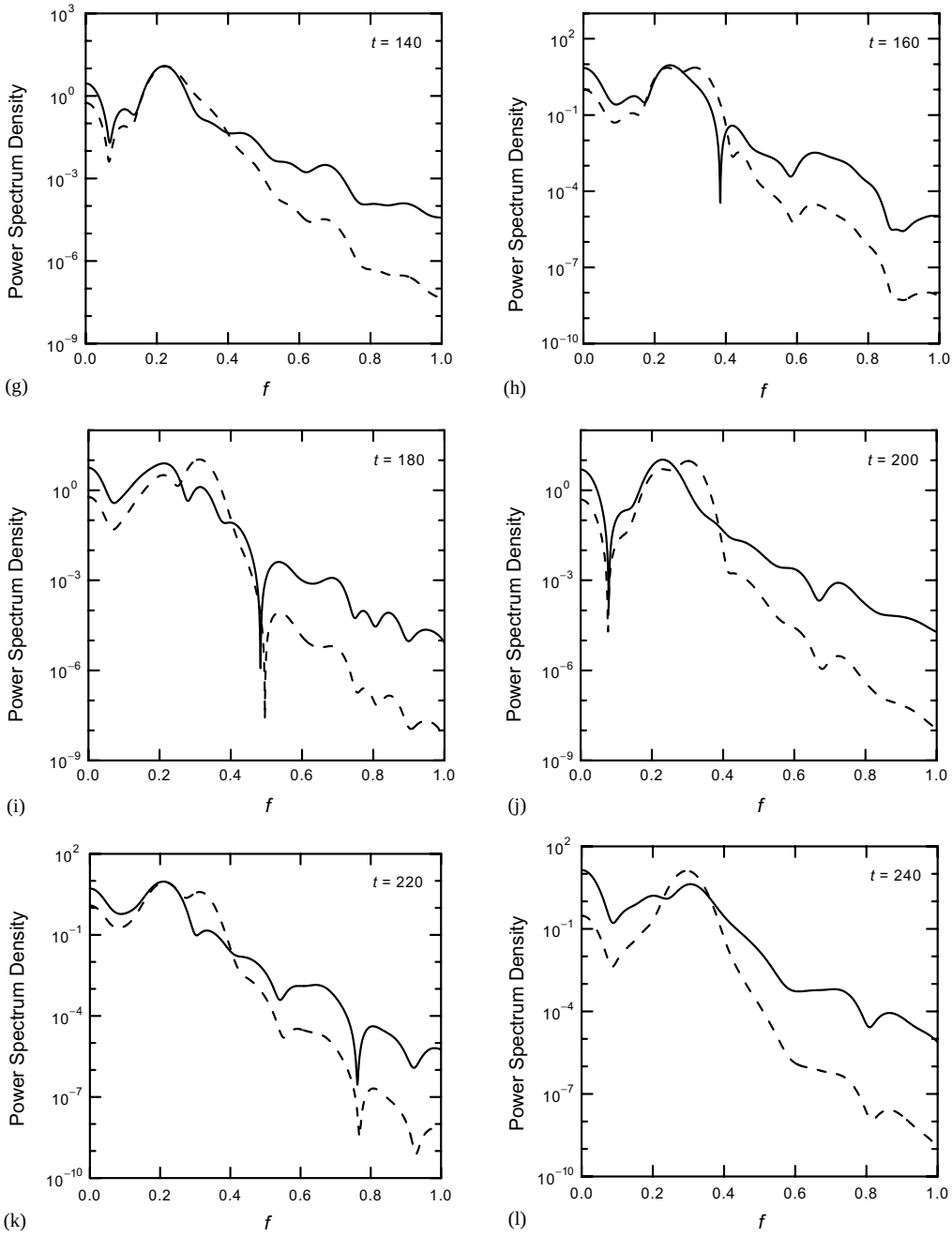


Figure 17. *Continued*

but a small peak at $f = 0{\cdot}33$ begins to appear. As $t$ increases to 240, the peak at $f = 0{\cdot}33$ becomes dominant and shifts to $f = 0{\cdot}31$, perhaps due to the effect of beam vibration, and the frequency at $f = 0{\cdot}21$ is reduced though still discernible at $f = 0{\cdot}20$. There is only one frequency peak at $f = 0{\cdot}30$ for $Y$ though. The behavior at $t = 260$ shifts back to that at $t = 200$, with only one dominant frequency at $f = 0{\cdot}20$. However, this frequency shifts to

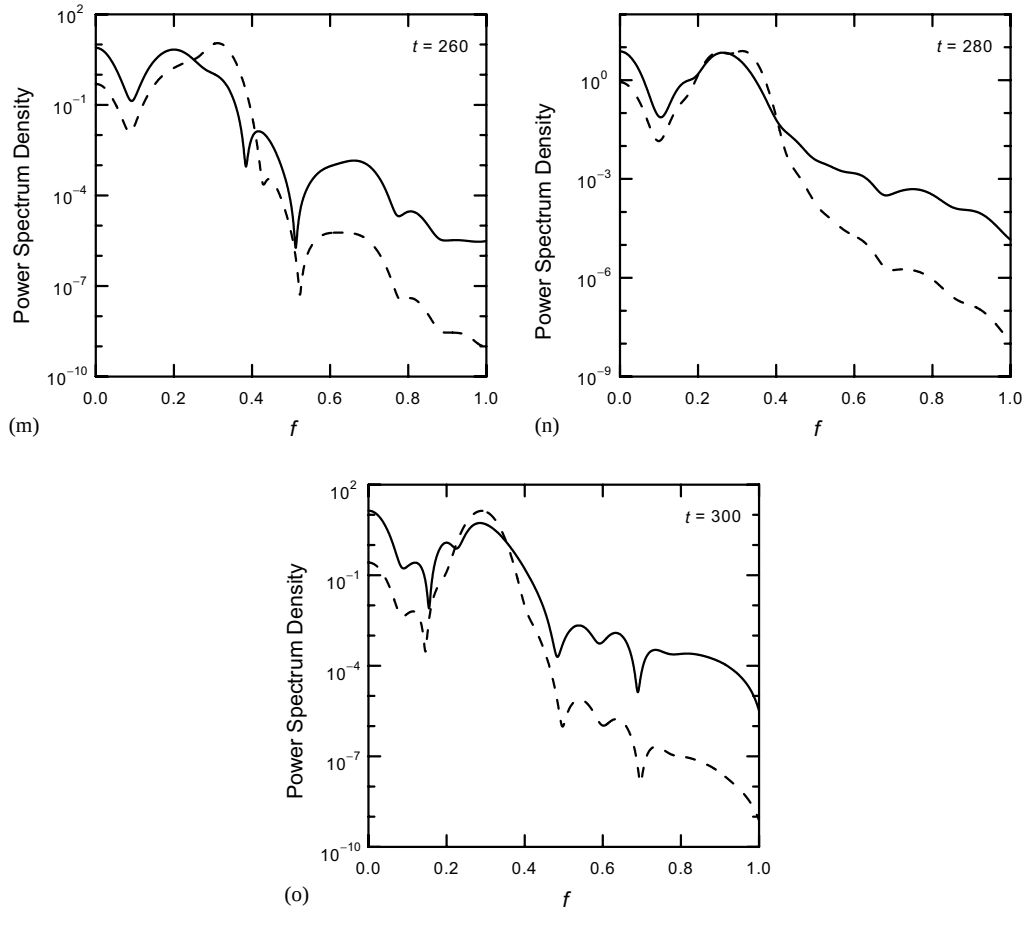


Figure 17. *Continued*

$f = 0{\cdot}26$ at $t = 280$, and then changes back to a behavior with three dominant frequencies at $f = 0{\cdot}12$, $0{\cdot}20$, and $0{\cdot}29$ as time increases to $t = 300$.

Through the above STFT analysis, it is seen that there are three types of time-variant frequency spectrum for $C_L$, that is, those with one, two, or three dominant frequencies. They can be labelled as Types A, B, and C, respectively, for convenience of discussion. For Type A, the single dominant frequency occurs at around $f = 0{\cdot}20$. For Type C, the three dominant frequencies can be found around $f = 0{\cdot}1$, $0{\cdot}2$ and $0{\cdot}3$. As for Type B, the two dominant frequencies occur at about $f = 0{\cdot}1$ and $0{\cdot}2$, or $0{\cdot}2$, and $0{\cdot}3$. This can be further classified as Types B1 and B2, respectively, depending on where the dominant frequencies are found. These three types of frequency spectrum change intermittently in a random way. It is interesting to note that a feature of three Strouhal numbers in the biased flow pattern regime has been reported in the literature [3, 5]. The present analysis suggests that such a feature is just one of the behavior of the non-stationary time series.

The ARMA calculated spectra of $C_L$ and $Y$ are plotted in Figure 18 for comparison with the STFT spectrograms. For $C_L$, one dominant frequency occurring at $f = 0{\cdot}23$ can be observed. Further analysis of the ARMA result shows there are two additional frequency peaks at $f = 0{\cdot}15$ and $0{\cdot}32$, although they are not discernible in the spectral plot. This is consistent with the feature of multiple Strouhal numbers reported in the literature.

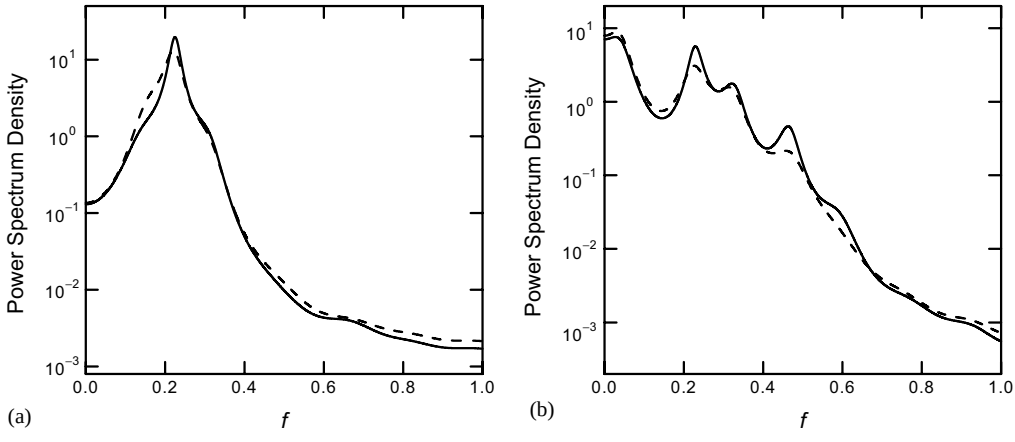


Figure 18. The ARMA deduced spectra for the $T/D = 1{\cdot}7$ case: (a) $C_L$; (b) $Y$, ——, beam 1; ------, beam 2.

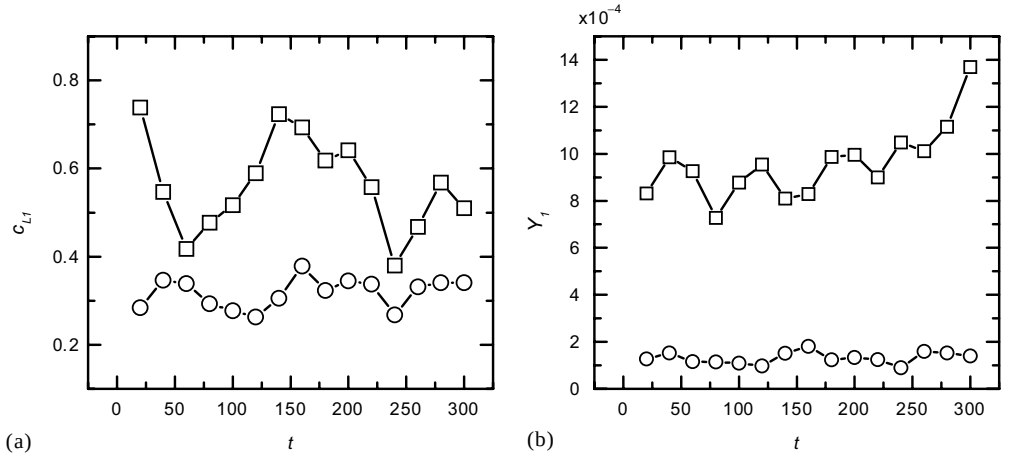


Figure 19. The time-dependent statistics of beam 1 for the $T/D = 1{\cdot}7$ case: (a) $C_L$; (b) $Y$; ⊖—⊖, mean value; □—□, r.m.s. value.

However, the present STFT analysis gives further insight about this feature as discussed above. As for the ARMA calculated spectrum of $Y$, the dominant frequencies occur at $f = 0{\cdot}23$ and $0{\cdot}31$. The response at the fundamental natural frequency is consistent with the STFT result, but the ARMA analysis cannot show the time variation of the response at the excitation frequency (frequencies).

In the STFT analysis, the complete data set is divided into a number of sections. The statistics of $C_L$ and $Y$ are calculated using these sections of data. The time-variant results are plotted in Figure 19. A comparison of the present result with experimental measurement and the numerical result from the 2-d.o.f. model is given in Table 4. It can be seen that $\bar{C}_{L1}$ agrees well with experimental measurement and the numerical result obtained from a 2-d.o.f. model. Also, $Y'_1$ agrees with the 2-d.o.f. numerical result, but is higher than the experimental measurement. These comparisons point to the danger of approximating the beam dynamics by a spring–damper–mass system without fully understanding the physics of the problem.

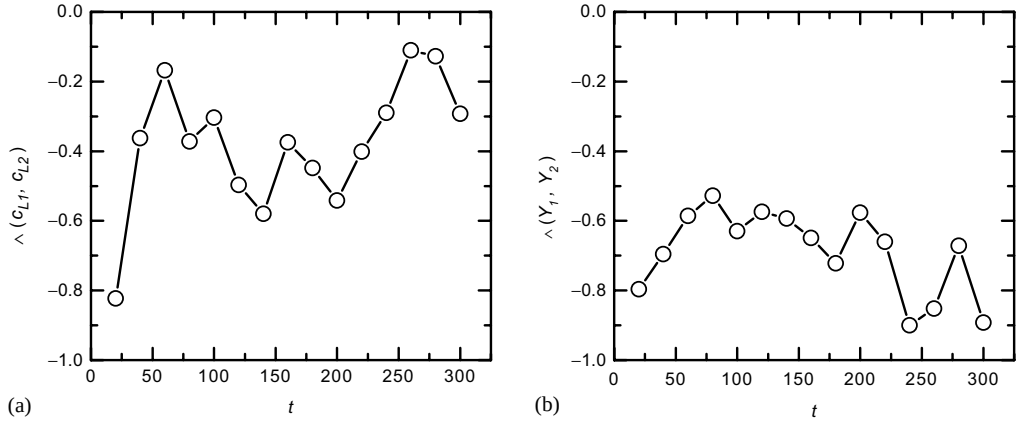


Figure 20. The time-dependent correlation coefficients between the two beams for the $T/D = 1{\cdot}7$ case: (a) $C_L$; (b) $Y$.

The variation of the correlation coefficient $\Lambda(C_{L1}, C_{L2})$ with time is plotted in Figure 20(a). All coefficients are negative, suggesting that the phase difference is between $\pi/2$ and $3\pi/2$. Except at $t = 20$, $\Lambda(C_{L1}, C_{L2})$ is randomly distributed in the range $-0{\cdot}1$ and $-0{\cdot}6$, that is, the phase difference between $0{\cdot}54\pi$ and $0{\cdot}70\pi$. The variation of the correlation coefficient $\Lambda(Y_1, Y_2)$ is plotted in Figure 20(b). They are also negative, but the value lies in the range $-0{\cdot}5$ and $-0{\cdot}9$, hence the phase difference is between $0{\cdot}67\pi$ and $0{\cdot}86\pi$.

## 4. CONCLUSIONS

Numerical simulation is used to study the free vibration of two side-by-side elastic beams in a cross flow at $\mathrm{Re} = 800$. In the numerical approach, the Navier–Stokes and the Euler–Bernoulli beam equations are used to model the complicated fluid–beam interaction problem. The finite element method combined with the modal analysis method is used to treat the equations. A time-marching technique is used to solve the resultant equations. Mesh remapping and iteration at every time step are invoked in order to resolve fluid–beam and beam–beam interactions in real time. The vibration of two beams at $T/D = 1{\cdot}13$, $1{\cdot}7$, and $3{\cdot}0$ is simulated. These $T/D$ ratios represent three different flow regimes for the side-by-side configuration. The short-time Fourier transform (STFT) method is used to analyze the time series, particularly for the biased flow regime occurring at $T/D = 1{\cdot}7$, where the conventional ARMA method is not applicable to the analysis of non-stationary time series.

The present results are compared with experimental measurements and another set of numerical results obtained from a 2-d.o.f. structural model. The agreement is good for some results, but only qualitatively for others. By comparing the present predictions with those obtained using a 2-d.o.f. structural model, it appears that the modelling of fluid flow in the present time-marching approach needs further improvements. The phase relationship between fluid forces and their corresponding vibration amplitudes of the two beams are also studied. For the regime of a single vortex street ($T/D = 1{\cdot}13$), an in-phase relation is observed. As for the regime of two coupled vortex streets ($T/D = 3{\cdot}0$), an out-of-phase relation is found. For the regime of biased flow ($T/D = 1{\cdot}70$), the phase difference varies with time, but falls into a certain range, between $0{\cdot}54\pi$ and $0{\cdot}70\pi$ for $C_L$, and between $0{\cdot}68\pi$ and $0{\cdot}86\pi$ for $Y$.

The STFT analysis shows that the vibration behavior at $T/D = 1{\cdot}13$ and $3{\cdot}0$ is stationary, while the vibration characteristics at $T/D = 1{\cdot}7$ is non-stationary. For the $T/D = 1{\cdot}13$ and $3{\cdot}0$ cases, the STFT results are consistent with the ARMA results. However, the STFT results clearly show the existence of even order harmonics in the spectra. For the $T/D = 1{\cdot}7$ case, the STFT analysis reveals that three types of frequency spectrum exist in the time series of $C_L$ or $Y$. These spectra intermittently change with time in a random way. This gives a new interpretation to the behavior in the biased flow regime. For this case, the STFT method is more suitable for the non-stationary time series deduced from the study of vortex-induced vibration.

## ACKNOWLEDGMENTS

Funding support from the Research Grants Council of the Government of the HKSAR under Grants PolyU5159/97E and PolyU5128/98E is gratefully acknowledged. Furthermore, X.Q.W. wishes to acknowledge support given to him in the form of a Research Fellowship by The Hong Kong Polytechnic University.

## REFERENCES

1. M. M. ZDRAVKOVICH 1977 *Transactions of the American Society of Mechanical Engineers Journal of Fluids Engineering*, **99**, 618–633. Review of flow interference between two circular beams in various arrangements.
2. M. M. ZDRAVKOVICH 1987 *Journal of Fluids and Structures* **1**, 239–261. The effects of interference between circular beams in cross flow.
3. P. W. BEARMAN and A. J. WADCOCK 1973 *Journal of Fluid Mechanics* **61**, 499–511. The interaction between a pair of circular beams normal to a stream.
4. C. H. K. WILLIAMSON 1985 *Journal of Fluid Mechanics* **159**, 1–18. Evolution of a single wake behind a pair of bluff bodies.
5. H. J. KIM and P. A. DURBIN 1988 *Journal of Fluid Mechanics* **196**, 431–448. Investigation of the flow between a pair of circular beams in the flopping regime.
6. M. M. ZDRAVKOVICH 1985 *Journal of Sound and Vibration* **101**, 511–521. Flow induced oscillations of two interfering circular beams.
7. S. S. CHEN 1986 *Transactions of the American Society of Mechanical Engineers Journal of Pressure Vessel Technology* **108**, 382–393. A review of flow-induced vibration of two circular beams in crossflow.
8. Y. ZHOU, Z. J. WANG, R. M. C. SO, S. J. XU and W. JIN 2001 *Journal of Fluid Mechanics* **443**, 197–229. Free vibrations of two side-by-side beams in a cross flow.
9. K. S. CHANG and C. J. SONG 1990 *International Journal for Numerical Methods in Fluids* **11**, 317–329. Interactive vortex shedding from a pair of circular beams in a transverse arrangement.
10. A. SLAOUTI and P. K. STANSBY 1992 *Journal of Fluids and Structures* **6**, 641–670. Flow around two circular beams by the random-vortex method.
11. C. W. NG, V. S. Y. CHENG and N. W. M. KO 1997 *Fluid Dynamics Research* **19**, 379–409. Numerical study of vortex interactions behind two circular beams in bistable flow regime.
12. T. ICHIOKA, Y. KAWATA, T. NAKAMURA, H. IZUMI, T. KOBAYASHI and H. TAKAMATSU 1997 *JSME International Journal Series B* **40**, 16–24. Research on fluid elastic vibration of beam arrays by computational fluid dynamics (analysis of two beams and a beam row).
13. X. Q. WANG, R. M. C. SO and Y. LIU 2001 *Journal of Sound and Vibration* **243**, 241–268. Flow-induced vibration of an Euler–Bernoulli beam.
14. Y. LIU, R. M. C. SO, Y. L. LAU and Y. ZHOU 2001 *Journal of Fluids Engineering*, (submitted). Multiple beams freely vibrating in a cross flow at sub-critical Reynolds numbers.
15. M. P. MIGNOLET and J. R. RED-HORSE 1994 *Proceedings of the 35th Structures, Structural Dynamics, and Materials Conference, American Institute of Aeronautics and Astronautics / American Society of Mechanical Engineers*, Hilton Head, South Carolina, April 18–20, 1628–1637. ARMAX identification of vibrating structures: model and model order estimation.

16. S. QIAN and D. CHEN 1996 *Joint Time–Frequency Analysis—Methods and Applications*. Upper Saddle River, NJ: Prentice-Hall PTR, Prentice-Hall Inc.
17. R. M. C. SO, Y. LIU, S. T. CHAN and K. LAM 2001 *Journal of Fluids and Structures* **15**, 845–866. Numerical studies of a freely vibrating beam in a cross flow.
18. R. GLOWINSKI and O. PIRONNEAU 1992 *Annual Review of Fluid Mechanics* **24**, 167–204. Finite element methods for Navier–Stokes equations.
19. L. MEIROVITCH 1997 *Principles and Techniques of Vibrations*. Englewood Cliffs, NJ: Prentice-Hall Inc.; International Edition.
20. I. JADIC, R. M. C. SO and M. P. MIGNOLET 1998 *Journal of Fluids and Structures* **12**, 631–654. Analysis of fluid–structure interactions using a time marching technique.
21. C. Y. ZHOU, R. M. C. SO and M. P. MIGNOLET 2000 *Journal of Fluids and Structures* **14**, 303–322. Fluid damping of an elastic beam in a cross flow.
22. R. M. C. SO, Y. ZHOU and M. H. LIU 2000 *Experiments in Fluids* **29**, 130–144. Free vibrations of an elastic beam in a cross flow and their effects on the near wake.
23. R. M. C. SO, Y. LIU and Y. ZHOU 2000 *Proceedings of the 7th International Conference on Flow-induced Vibration—FIV* 2000, *Lucerne*, *Switzerland*, June 19–22, 97–104. Fluid–structure interactions of two side-by-side circular beams.